

AD-A179 733

ON THE THREE-DIMENSIONAL STRUCTURE OF BOUNDARY LAYERS
UNDERGOING TRANSITI. (U) VIRGINIA POLYTECHNIC INST AND
STATE UNIV BLACKSBURG W S SARIC MAR 85

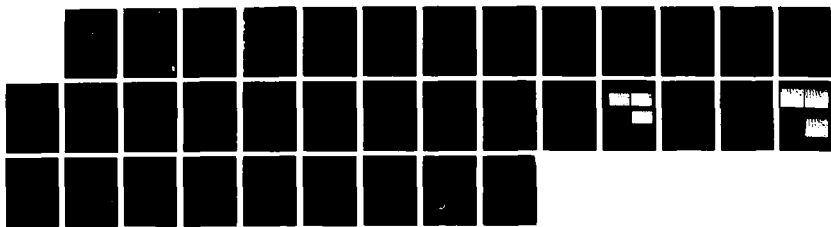
1/1

UNCLASSIFIED

AFOSR-TR-87-0393 AFOSR-82-0299

F/G 28/4

NL





MI

UNCLASSIFIED

AD-A179 733

DTIC FILE COPY

2

REPORT DOCUMENTATION PAGE

1a. REPORT SECURITY CLASSIFICATION UNCLASSIFIED		1b. RESTRICTIVE MARKINGS										
2a. SECURITY CLASSIFICATION AUTHORITY		3. DISTRIBUTION/AVAILABILITY OF REPORT APPROVED FOR PUBLIC RELEASE DISTRIBUTION IS UNLIMITED										
2b. DECLASSIFICATION/DOWNGRADING SCHEDULE												
4. PERFORMING ORGANIZATION REPORT NUMBER(S)		5. MONITORING ORGANIZATION REPORT NUMBER(S) AFOSR-TR- 87-0393										
6a. NAME OF PERFORMING ORGANIZATION VIRGINIA POLYTECHNIC INSTITUTE AND STATE UNIVERSITY	6b. OFFICE SYMBOL (If applicable)	7a. NAME OF MONITORING ORGANIZATION AFOSR/NA										
8a. ADDRESS (City, State and ZIP Code) VPI SU BLACKSBURG VA 24061		7b. ADDRESS (City, State and ZIP Code) BUILDING 410 BOLLING AFB, DC 20332-6448										
8b. NAME OF FUNDING/SPONSORING ORGANIZATION	8b. OFFICE SYMBOL (If applicable)	9. PROCUREMENT INSTRUMENT IDENTIFICATION NUMBER AFOSR-82-0229										
10. ADDRESS (City, State and ZIP Code) BUILDING 410 BOLLING AFB, DC 20332-6448		10. SOURCE OF FUNDING NOS <table border="1"> <tr> <td>PROGRAM ELEMENT NO 61102F</td> <td>PROJECT NO. 2307</td> <td>TASK NO. K1</td> <td>WORK UNIT NO.</td> </tr> <tr> <td colspan="4">LAYERS</td> </tr> </table>		PROGRAM ELEMENT NO 61102F	PROJECT NO. 2307	TASK NO. K1	WORK UNIT NO.	LAYERS				
PROGRAM ELEMENT NO 61102F	PROJECT NO. 2307	TASK NO. K1	WORK UNIT NO.									
LAYERS												
11. TITLE (Include Security Classification) (U) ON THE 3-D STRUCTURE OF BOUNDARY LAYERING TRANSITION TO TURBULENCE												
12. PERSONAL AUTHORITY W. SAKIC												
13a. TYPE OF REPORT FINAL	13b. TIME COVERED FROM _____ TO _____	14. DATE OF REPORT (Yr., Mo., Day) MAR 1985	15. PAGE COUNT 33									
16. SUPPLEMENTARY NOTATION												
17. COSATI CODES <table border="1"> <tr> <th>FIELD</th> <th>GROUP</th> <th>SUB GR</th> </tr> <tr> <td> </td> <td> </td> <td> </td> </tr> <tr> <td> </td> <td> </td> <td> </td> </tr> </table>		FIELD	GROUP	SUB GR							18. SUBJECT TERMS (Continue on reverse if necessary and identify by block number) TRANSITION, BOUNDARY LAYER, TURBULENCE	
FIELD	GROUP	SUB GR										
19. ABSTRACT (Continue on reverse if necessary and identify by block number) <p>Detailed experiments were performed for boundary layers undergoing transition to turbulence. The experiments utilized multiple hot wire anemometer techniques in combination with recently developed flow visualization and computational techniques. The use of a phase-correlated and conditionally sampled measurements permitted the study of the origin and evolution of the characteristic of transitional boundary layers. Fundamental transition mechanisms and the receptivity of the boundary layer to external disturbances that led to transition were studied.</p> <p style="text-align: center;">(U)</p>												
20. DISTRIBUTION/AVAILABILITY OF ABSTRACT UNCLASSIFIED/UNLIMITED <input checked="" type="checkbox"/> SAME AS RPT <input type="checkbox"/> DTIC USERS <input type="checkbox"/>		21. ABSTRACT SECURITY CLASSIFICATION APR 27 1987 UNCLASSIFIED										
22a. NAME OF RESPONSIBLE INDIVIDUAL HENRY E HELIN, CAPTAIN, USAF		22b. TELEPHONE NUMBER (Include Area Code) 202-767-4935	22c. OFFICE SYMBOL AFOSR/NA									

AFOSR-TR- 87-0393

FINAL REPORT

ON THE THREE-DIMENSIONAL STRUCTURE OF BOUNDARY
LAYERS UNDERGOING TRANSITION TO TURBULENCE

To

Air Force Office of Scientific Research
Bolling Air Force Base
Washington D.C. 20332

Approved for public release;
distribution unlimited.

For

CONTRACT NO. AFOSR-82-0299
AT VIRGINIA POLYTECHNIC INSTITUTE & STATE
UNIVERSITY

AIR FORCE OFFICE OF SCIENTIFIC RESEARCH (AFSC)
NOTICE OF TRANSMITTAL TO DTIC
The technical report has been reviewed and is
approved for public release IAW AFR 190-12.
Distribution unlimited.
MATTHEW S. SARIC
Chief, Technical Information Division

By

WILLIAM S. SARIC
Professor

Mechanical and Aerospace Engineering
Arizona State University
Tempe, AZ 85287

March 1985



Accession For	
NTIS GRA&I	
DTIC TAB	
Unannounced	
Justification	
A	
By _____	
Distribution/	
Availability Codes	
Dist	Avail and/or Special
A-1	

87 4

ABSTRACT

The final report for Contract AFOSR-82-0299 is given. Detailed experiments were performed of boundary layers undergoing transition to turbulence. The experiment utilized multiple hot-wire anemometer techniques in combination with recently developed flow visualization and computational techniques. The use of phase-correlated and conditionally-sampled measurements permitted the study of the origin and evolution of the characteristic large-scale structures of transitional boundary layers. Fundamental transition mechanisms and the receptivity of the boundary layer to external disturbances that lead to transition were studied.

This work represents the most detailed study of the subharmonic transition mechanism in boundary layers and in both natural and controlled situations. It laid the foundation for more advanced work in boundary-layer transition and control.

TABLE OF CONTENTS

1. ACCOMPLISHMENTS.....	1
1.1 Presentations.....	1
1.2 Publications.....	2
2. TECHNICAL DISCUSSION.....	3
2.1 Nomenclature.....	3
2.2 Introduction.....	4
2.3 Motivation.....	6
2.4 Description of the Experiments.....	7
2.5 Results.....	10
3. CONCLUSIONS.....	17
4. REFERENCES.....	18
5. FIGURES.....	20 - 30

2.0 TECHNICAL DISCUSSION

2.1 Nomenclature

a = $(\alpha/R) \times 10^3$: normalized chordwise wavenumber
 b = $(\beta/R) \times 10^3$: normalized spanwise wavenumber
 F = $(2\pi\nu f/U^2) \times 10^6$: dimensionless frequency
 \hat{F} = $F/2$: subharmonic frequency
 f = dimensional frequency (hz)
 R = $U\delta_r/\nu = \sqrt{R_x}$: boundary-layer Reynolds number
 R_x = Ux_v/ν : x -Reynolds number
 U = freestream velocity
 u = mean boundary-layer velocity normalized with
 u' = $|u'|/U$: r.m.s. of fundamental fluctuating velocity in
chord direction normalized with U
 \hat{u}' = $|\hat{u}'|/U$: r.m.s. of subharmonic component
 x = dimensional distance in chord direction (from leading
edge)
 x_v = $0.338 \delta^{*2} U/\nu$: virtual distance from leading edge
based on displacement-thickness measurement
 y = dimensional distance normal to plate
 z = dimensional spanwise distance (from centerline)
 α = $2\pi\delta_r/\lambda_x$: dimensionless chordwise wavenumber
 β = $2\pi\delta_r/\lambda_z$: dimensionless spanwise wavenumber
 δ_r = $(\nu x_v/U)^{1/2}$: boundary-layer reference length
 δ^* = displacement thickness
 θ = $\arctan(2\lambda_x/\lambda_z)$: wave angle
 λ_x = dimensional chordwise wavelength
 λ_z = dimensional spanwise wavelength

1.2 Publications

"Computer controlled Wind Tunnel Experiments: Part I. Peak-
Valley Splitting of Unstable waves," R. W. Henk and W. S. Saric,
V.P.I. & S.U. Report No. VPI-E-83.24, June 1983.

"Forced and Unforced Subharmonic Resonance in Boundary-Layer
Transition," W. S. Saric, V. V. Kozlov and V. Ya. Levchenko, AIAA
Paper No. 84-0007, AIAA Aerospace Sciences Meeting, Reno, Nevada,
January 9-12, 1984. Submitted to AIAA Journal.

ν = kinematic viscosity

ϕ = relative phase between fundamental and subharmonic

$\hat{\cdot}$ = denotes subharmonic

2.2 Introduction

The understanding and ultimate control of turbulent boundary layers are goals with important roles in determining the performance characteristics of flight vehicles. A part of the progress toward these goals is the understanding of the basic mechanisms of boundary-layer transition to turbulence. There are different possible scenarios for the transition process, but it is generally accepted that transition is the result of the uncontrolled growth of unstable three-dimensional waves.

The occurrence of three-dimensional phenomena in an otherwise two-dimensional flow is a necessary prerequisite for transition. Such phenomena were observed in detail by Klebanoff et al.¹ and were attributed to a spanwise differential amplification of Tollmien-Schlichting (T-S) waves through corrugations of the boundary layer. The process led rapidly to spanwise alternating "peaks" and "valleys", i.e., regions of enhanced and reduced wave amplitude, and an associated system of streamwise vortices. The peak-valley structure evolved at a rate much faster than the (viscous) amplification rates of T-S waves. The smoke-streakline photograph² in Figure 1 clearly shows the rapid sequence of events after the onset of "peak-valley splitting". The unstable waves are observed to be two-dimensional until the 160 cm location when the pattern breaks

down very quickly. This represents the path to transition under conditions similar to Klebanoff et al.¹ and is called a K-type breakdown. The Λ shaped³ spanwise corrugations of streaklines, which correspond to the peak-valley structure of amplitude variation, are a result of weak 3-D displacements of fluid particles across the critical layer and precede the appearance of Klebanoff's "hair-pin" vortices. This has been supported by hot-wire measurements and a Lagrangian-type streakline prediction code². Note that the Λ vortices are ordered in that peaks follow peaks and valleys follow valleys.

Different types of three-dimensional transition phenomena recently observed (see References 2,4-10) are characterized by staggered patterns of peaks and valleys (see Fig. 2 and 3) and by their occurrence at very low amplitudes of the fundamental T-S wave. This pattern also evolves rapidly into transition. These experiments showed that the subharmonic of the fundamental wave (a necessary feature of the staggered pattern) was excited in the boundary layer and produced either the resonant wave interaction predicted by Craik¹¹ (Fig. 2) called the C-type or the secondary instability of Herbert¹² (Fig. 3) called the H-type. Spectral broadening to turbulence with self-excited subharmonics has been observed in acoustics, convection, and free shear layers and was not observed in boundary layers until the results of Kachanov et al.⁴. They initiated the interest in subharmonics and prompted the simultaneous verification of C-type resonance^{2,5,6}. Subharmonics have also been confirmed for channel flows¹³. This work is reviewed by Saric and Thomas⁷ and Levchenko⁸, and the

background for this paper can be found there. The recent theoretical treatment is given by Herbert¹⁴.

2.3 Motivation

When the source of the 3-D subharmonic is the background disturbance environment, then two such subharmonics (different in phase by 180°) can be phase locked with the fundamental⁶. Since the background disturbances are random to some extent, phase synchronization randomly alternates between these two waves and thus accounts for the spectral broadening of the subharmonic. This contributes to a definite unsteadiness in the signals being measured. Moreover, a long fetch (distance from the vibrating ribbon) is required to phase-lock and entrain the subharmonic from the background so that its amplitude is of the order of the fundamental. It has been our experience that the three-dimensionality of long-fetch waves is inherently unsteady whether one deals with C-, H-, or K-type interactions. The unsteadiness appears as a spanwise meandering of the peak-valley structure and is a characteristic of wind tunnels with very low turbulence levels (0.02%-0.03%). Thus, there are two courses of unsteadiness when dealing with naturally occurring disturbances interacting with a primary wave. In order to compare with theoretical models, it is necessary to make detailed measurements of the disturbances under steady conditions.

In order to achieve a steady occurrence of the subharmonic resonance, a signal of one-half the frequency of the fundamental is introduced on the vibrating ribbon. This is done using the

same technique as Saric and Reynolds¹⁵. Thus, two 2-D waves at F and $\frac{1}{2}F$ are introduced into the boundary layer. The symbol \wedge will always denote the subharmonic at $F/2$. The relative amplitude and phase are accurately controlled be separately computing the signals on a DEC-MINC-11/23 computer and D/A converting. The appropriate 3-D subharmonic then evolves from the 2-D subharmonic. Under certain conditions, it is possible to obtain spatially-steady resonance. The results are described below.

2.4 Description of the Experiments

The experiments are performed in the VPI & SU Stability Wind Tunnel. The facility is a closed-loop tunnel having a 9:1 contraction ratio to the test section which is 1.83 m square and 7.31 m long. Seven turbulence damping screens are located in the settling chamber; these screens have an open-area ratio of 0.6. The flow is driven by a 4.3 m diameter fan which has eight constant-pitch blades. Turning vanes are located at each corner of the flow loop; those vanes located the in the settling chamber are spaced every .076 m to help reduce any large-scale turbulence in the flow. The resulting flow in the test section is very uniform and steady with a turbulence level of $u' = 0.02\%$ at velocities of 16 m/s. The spectrum of the freestream turbulence shows virtually all of the energy below 20 hz. The zero-pressure-gradient flat-plate transition Reynolds number is $R_x = 3.4 \times 10^6$ at $U = 20$ m/s. Transition is defined as the chordwise location where the sign of du/dx at fixed y first changes from negative to positive.

The model is a flat-plate having a 1.83 m span, 4 m chord and 0.021 m thickness placed at an angle-of-attack of 0.25° to account for blockage. A variable-deflection trailing-edge flap is installed on the downstream end of the flat plate in order to control the position of the attachment line on the leading edge. A carefully contoured leading edge is used which has an elliptical profile with a major-to-minor axis ratio of 67:1. Chordwise and spanwise static pressure measurements are made by a total of 91 static pressure ports which are imbedded in the surface of the plate along two chordwise and spanwise arrays. Differential pressures are measured via scanivalves and a ± 0.5 mm Hg differential-pressure transducer. Except for the region near the leading edge, the model has essentially a zero pressure gradient.

Disturbances are introduced into the boundary layer by means of a vibrating ribbon. The ribbon is made of phosphor-bronze, 0.025 mm thick, 2.5 mm wide, with a span of 380 mm. It is mounted 0.3 mm from the surface at a tension of 25 N which gives a natural frequency in the range of 200 hz. A stainless steel ribbon is also used with a span of 800 mm and a tension of 45 N in order to avoid the effects predicted by Mack¹⁶. The results are unchanged by this new configuration except that the T-S amplitudes are more nearly uniform over a greater span. Measurements of ribbon amplitude, phase, and frequency content are accomplished by means of an inductance probe which is flush mounted on the surface of the plate beneath the ribbon. The

initial amplitudes of the fundamental and subharmonic on the vibrating ribbon are always recorded.

A three-dimensional traversing mechanism driven by stepping motors is used to traverse 3.7 m along the chord of the plate, 0.2 m along the span, and 0.1 m normal to the plate. The minimum step sizes in the chordwise, spanwise, and normal directions are 0.6 mm, 0.03 mm, and 0.02 mm respectively. The x- and z-traverse directions are controlled manually, whereas the y-traverse direction (normal to the plate) is controlled by the data-acquisition-system controller. The traverse position is monitored by keeping a binary count of motor pulses. This count is D/A converted to provide a d.c. voltage to the data-acquisition input board.

The data collection and processing are handled through a HP 3052A data-acquisition system. This system makes d.c. and r.m.s. measurements in a serial fashion from the various instruments in the experiment and provides processing for output purposes. Two-channel spectral analysis is accomplished using a HP 5420A digital signal analyzer which is also interfaced to the data-acquisition-system controller.

The measurements of mean-flow velocity and disturbance velocity in the boundary layer are made almost exclusively by hot-wire anemometry. DISA anemometers and linearizers are used and operated in the constant-temperature mode. Three channels of anemometry are available for simultaneous measurement of various quantities or for spatial measurements of the same quantity. In general, however, single-point measurements are sufficient to

study the behavior of the waves. These instruments are accompanied by the usual assortment of tracking filters, differential amplifiers, phase meters, and r.m.s. meters. Oscillating signals to the vibrating ribbon are generated digitally on the MINC 11/23.

2.5 Results

A. Natural Subharmonic

Figure 4 is the neutral stability loop for the Blasius boundary layer upon which is shown the location of the vibrating ribbon and smoke wire for air at $U = 7.5 \text{ m/s}$ and $\nu = 15 \times 10^{-6} \text{ m}^2/\text{s}$. The constant frequency line $F=76$ corresponds to the fundamental at 45.5 hz, and single-frequency measurements are confined over the length of this line. All of the reported data with natural subharmonics are presented for these conditions. Also shown is the experimentally determined branch II neutral stability point at $u=0.4$.

Figure 5 shows the disturbance amplitude growth in the chord direction for the fundamental with four different initial amplitudes, u' , at the reference point of $R_0 = 550$. In each case the Reynolds number of the measurement is determined from the displacement thickness obtained from an integration of the local velocity profile. The virtual leading edge in this case is an almost constant 10 cm downstream of the actual leading edge. All amplitude measurements are made at the distance from the wall where $u=0.4$. The amplitude curve associated with $u'=0.028\%$ shows a branch II neutral point at $R=920$ which compares well with

linear theory. A dog-leg in the amplitude curve occurs just aft of the location of the smoke wire. It is found^s that the smoke wire produces a local kink in the velocity profile which locally amplifies the T-S wave at a rate much higher than the usual viscous growth rate. This effect heals 8-10 cm (30-40 δ *) downstream of the smoke wire, and thereafter the T-S wave is "normal" in every respect. One could also use the amplitude $u'=0.16\%$ at $R_1=710$ as the normalizing amplitude and avoid referencing conditions upstream of the smoke wire. In this case it makes little difference. As R approaches 1000, the signal becomes unsteady and three-dimensionality appears.

The amplitude curve associated with $u'=0.038\%$ exhibits the C-type breakdown near $R=1000$. The relative amplitude appears to drop below the previous lower-amplitude curve due to the interaction of the subharmonic (whose amplitude curve is also shown in this case). However, the signal is unsteady, and the error bars on the data show the magnitude of the fluctuation. The C-type breakdown is confirmed by flow visualization as shown in Fig. 6. The reference amplitude at $R_1=710$ is $u'=0.23\%$, and the normalized spanwise wavenumber is $b=0.14\pm 0.01$ with the ratio of wave-numbers given by $b/a=0.7$.

The amplitude curve associated with $u'=0.06\%$ exhibits the H-type breakdown as confirmed by the flow visualization shown in Fig. 7. Note the staggered structure with the smaller spanwise wavelength. In this case we see the H-type breakdown occur within the neutral stability loop and at amplitudes slightly

higher than those observed by Kachanov and Levchenko⁶ and Saric and Thomas⁷. Here $u' = 0.3\%$ and $b = 0.2$ with $b/a = 1.0$. As the amplitude is increased further to $u' = 0.09\%$, the flow goes to a K-type breakdown as shown in Fig. 8. Here we have the ordered peak-valley configuration.

The error bars on the data indicate the degree to which the signal is unsteady due to spanwise meandering of the 3-D structure. Any attempts made to steady the signal by the use of cellophane tape at the observed wavelength do not work. As mentioned earlier, this is due to the long fetch of the waves, the very low background-disturbance levels, and by resonance with two subharmonics different in phase by 180° . The K-type breakdown can be made steady by a further increase in amplitude so that it occurs closer to the vibrating ribbon. However, the subharmonic resonances with natural disturbances require a long fetch^{5,7}.

B. Controlled Subharmonic

The preceding section describes the usual sequence of events with natural subharmonics^{7,8}. The next series of results were obtained by directly introducing the subharmonic at the vibrating ribbon with the goal of achieving steady signals. The neutral stability loop (Fig. 4) shows the constant frequency line at $F = 106$ corresponding to a fundamental at 64.2 hz. The experimental branch II point is shown and as before $U = 7.5$ m/s, and the measurements were confined over the length of the constant frequency line. The subharmonic at $\hat{F} = 53$ is shown as a

dashed line, and the experimentally determined branch I neutral point is shown for $u=0.39$. The choice of F is dictated in large measure to the position of the vibrating ribbon with respect to the neutral stability curve, the type of measurements being conducted, idealization of flow-visualization conditions, and whether steady conditions can be obtained. For our conditions it is better to do the free subharmonic at a fundamental frequency of $F=76$ and the forced subharmonic at a fundamental frequency of $F=106$. The forced data at $F=106$ are close to those of ref. 6.

Figure 9 shows three amplitude curves measured at the distance from the wall where $u=0.39$ and at a spanwise location of $z=-2$ cm (more on this later). The curve with open circles, \hat{F} only, shows the growth of the input subharmonic in the absence of fundamental F . The amplitude at $R=630$ is used as a reference point. The usual growth of the 2-D wave is indicated with the step in the neighborhood of the smoke wire. When the input signal is $F + \hat{F}$, the component at \hat{F} shown with closed symbols, grows more rapidly while the fundamental, which should begin to decay at $R=700$, also continues to grow. The eventual breakdown occurs with the C-type mechanism with a spanwise wavelength of $\lambda_z = 6.5$ cm. This corresponds to spanwise wavenumber of $b=0.20$ and a chordwise wavenumber $a=0.27$ where $b/a=0.72$. The wave angle θ is defined as $\theta = \arctan (2\lambda_x/\lambda_z)$ where $\lambda_x/\lambda_z = b/a$. For the data obtained in these experiments, $\theta \approx 55^\circ$ which compares well with $\theta \approx 63^\circ$ at higher frequencies⁶ and $\theta \approx 53^\circ$ at lower frequencies⁷, both obtained for natural disturbances. The appearance of the C-type breakdown occurs in a relatively small range of low

amplitude conditions where the spanwise wavenumber is characteristic of 3-D, subharmonic Orr-Sommerfeld modes with the same phase speed as the fundamental. An increase in amplitude produces a 30-40% change in the spanwise wavenumber, and the 3-D, subharmonic Orr-Sommerfeld mode does not have the same phase speed. The Squire modes¹⁴ do, and their spanwise wavenumber changes continuously as the amplitude is increased in the same way as the theory¹⁴ predicts.

The spectra of the disturbances at $R=770$, shown in Fig. 10, is illustrative of the cleanness of the controlled subharmonic environment. The curve labeled $F+\hat{F}$ illustrates sharp peaks at \hat{F} , F , $3\hat{F}$, $2F$, etc. in contrast to the rather broad peaks reported by refs. 4-6. If the subharmonic is turned off and the amplitude of the fundamental raised to the $F+\hat{F}$ case, we see a spectrum characteristic of the K-type breakdown. When the fundamental is turned off and only \hat{F} remains, nothing much happens in the way of transition and our constant friend at 60 hz (and its multiples) become more noticeable.

In the results of Fig. 9 the relative phase, ϕ , between the fundamental and the subharmonic (at the output from the vibrating ribbon) is kept at zero.* Figure 11 shows three amplitude curves in the same manner as Fig. 9, except the relative phase is 90° . Note how the fundamental passes through the branch II neutral point in the usual manner and that the fundamental and subharmonic show no evidence of interacting until $R>740$. We see

*The ribbon acts as a low-pass filter, and the two-channel D/A is not exactly simultaneous. These contribute to phase shifts along the transmission. Therefore, the ribbon output measured from the proximeter probe is used for phase determination.

that the initial relative phase between the fundamental and subharmonic strongly effects the conditions for resonance.

Figure 12 shows the effect of relative phase on the amplitudes of the subharmonic and fundamental under the conditions of the last two figures. This effect is brought out even more dramatically in Fig. 13 where the initial amplitude of the subharmonic is greater than the previous cases. Very rapid growth of the subharmonic occurs between $R=725$ and $R=742$ when $\phi=0^\circ, 180^\circ, 360^\circ$ and a rather benign situation exists when $\phi=90^\circ, 270^\circ$.

The spanwise amplitude and phase variations of the subharmonic are shown in Figs. 14 and 15. In each figure the solid symbol indicates the position of the 180° phase shift. Here $\hat{\phi}$ represents the actual phase of the measured subharmonic with respect to a reference point. The obvious peak at $z=-2\text{cm}$ determines the span location of the amplitude measurements. With measurements such as this, it is easy to determine the spanwise wavelength. Spanwise measurements of the fundamental also show a spanwise periodic variation.

The mechanism for exciting the 3-D subharmonic with the 2-D initial conditions is not yet clear. Figure 16 gives the \hat{u} profiles at $R=630$ and $R=775$. The measurement at $R=775$ has all of the indications of the 3-D wave at those conditions¹⁴. The 3-D wave-amplitude distribution is typically characterized by a peak near $u=0.4$, hence the choice of the location to measure the amplitudes of Figs. 5, 9, 11. The measurement at $R=630$ looks as though it is not a completely 2-D or completely 3-d wave but a

combination of both. The 2-D wave-amplitude distribution is characterized by a sharp peak near $u=0.2$. The unusual spanwise modulation of \hat{u} shown in Fig. 14 could also be a result of a combination of 2-D and 3-D waves since the 3-D wave has not yet grown too large at this location. Both the vibrating ribbon and the smoke wire have a finite span, and that may be sufficient to create three-dimensionality except that both the ribbon and the wire are placed symmetrically about the plate centerline and one must recognize the asymmetry of Figs. 14 and 15. Moreover, increasing the span of the ribbon by a factor of 2.1 and eliminating the smoke wire does not change the general nature of the behavior. More than likely, the 3-D waves are synchronized through a parametric resonance between the 2-D subharmonic and the 3-D background subharmonic. Thus, another face of the receptivity question is bared.

3. CONCLUSIONS

It is shown that it is possible to model the naturally occurring subharmonic resonance by forcing the subharmonic at the vibrating ribbon with careful amplitude and phase control. The relative phase between the fundamental and subharmonic is shown to be important in both the natural and controlled interaction. It is found that over some narrow window of parameters, this technique reduces the unsteadiness of the interaction. It is now possible to proceed with measurements in the later stages of nonlinear breakdown with the use of simple conditional sampling techniques.

4. REFERENCES

¹Klebanoff, P. S., Tidstrom, K. D. and Sargent, L. M., "The Three-Dimensional Nature of Boundary-Layer Instability," Journal of Fluid Mechanics, 12, 1962, pp. 1-34.

²Saric, W. S., Carter, J. D. and Reynolds, G. A., "Computation and Visualization of Unstable-Wave Streaklines in a Boundary Layer," Bulletin of American Physical Society, 26, 1981, p. 1252.

³Hama, F. R. and Nutant, J., "Detailed Flow-Field Observations in the Transition Process in a Thick Boundary Layer," Proceedings of the 1963 Heat Transfer and Fluid Mechanics Institute, pp. 77-87.

⁴Kachanov, Yu. S., Kozlov, V. V. and Levchenko, V. Ya., "Nonlinear Development of a Wave in a Boundary Layer" (in Russian), Mekhaniki Zhidkosti i Gaza, 3, 1977, pp. 49-53.

⁵Thomas, A. S. W. and Saric, W. S., "Harmonic Subharmonic Waves During Boundary-Layer Transition," Bulletin of American Physical Society, 26, 1981, p. 1252.

⁶Kachanov, Yu. S. and Levchenko, V. Ya., "Resonant Interactions of Disturbances in Transition to Turbulence in a Boundary Layer" (in Russian), Preprint No. 10-82, ITAM, USSR Academy of Sciences, Novosibirsk, 1982.

⁷Saric, W. S. and Thomas, A. S. W., "Experiments on the Subharmonic Route to Turbulence in Boundary Layers," Proceedings IUTAM Symposium on Turbulence and Chaotic Phenomena in Fluids, Kyoto, Japan, September 5-12, 1983.

⁸Levchenko, V. Ya., "Resonance Phenomena at Laminar-Turbulent Transition in Boundary Layers," Proceedings IUTAM Symposium on Turbulence and Chaotic Phenomena in Fluids, Kyoto, Japan, September 5-12, 1983.

⁹Hama, F. R., "Some Transition Patterns in Axisymmetric Boundary Layers," Physics of Fluids, 2, 1959, pp. 664-667.

¹⁰Knapp, C. F. and Roache, P. J., "A Combined Visual and Hot-Wire Anemometer Investigation of Boundary-Layer Transition," AIAA Journal, 6, 1968, pp. 29-36.

¹¹Craik, A. D. D., "Nonlinear Resonant Instability in Boundary Layers," Journal of Fluid Mechanics, 50, 1971, pp. 393-413.

¹²Herbert, Th., "Subharmonic Three-Dimensional Disturbances in Unstable Plane Shear Flows," AIAA Paper 83-1759, 1983.

¹³Kozlov, V. V. and Ramazanov, M. P., "Development of Finite Amplitude Disturbances in a Poiseuille Flow (in Russian)," Mekhaniki Zhidkosti i Gaza, 1983, pp. 43-47, and private communications November 1982.

¹⁴Herbert, Th., "Analysis of the Subharmonic Route to Transition in Boundary Layers," AIAA Paper 84-0009, 1984.

¹⁵Saric, W. S. and Reynolds, G. A., "Experiments on the Nonlinear Stability of Waves in a Boundary Layer," In: Laminar-Turbulent Transition, R. Eppler and H. Fasel, eds., Springer-Verlag, 1980.

¹⁶Mack, L. M., "Line Sources of Instability Waves in a Blasius Boundary Layer," AIAA Paper 84-0168, 1984.

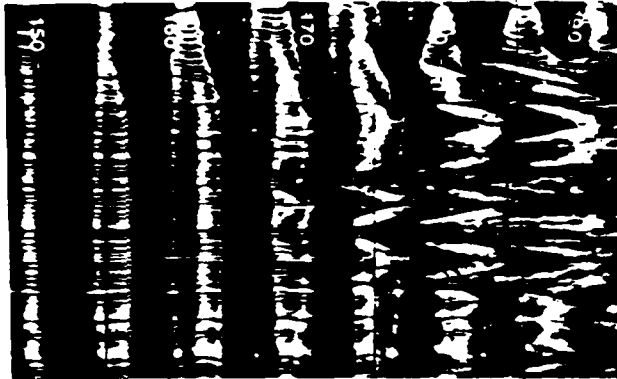


Figure 1. K-type breakdown. The distance from the leading edge is shown in cm. The vibrating ribbon is at $x=48$ cm. The smoke wire is at $x=138$ cm which is a Reynolds number $R=784$. Branch II for dimensionless frequency $F=83$ is $x=170$ cm ($R=870$). For this case $U_\infty=6.6$ m/s and $f=39$ hz. The chordwise wavenumber $a = a/R \times 10^3 = 0.22$. The spanwise wavenumber is $b = b/R \times 10^3 = 0.33$. $b/a = 1.5$. Maximum rms u' amplitude at Branch II is approx. 1%.

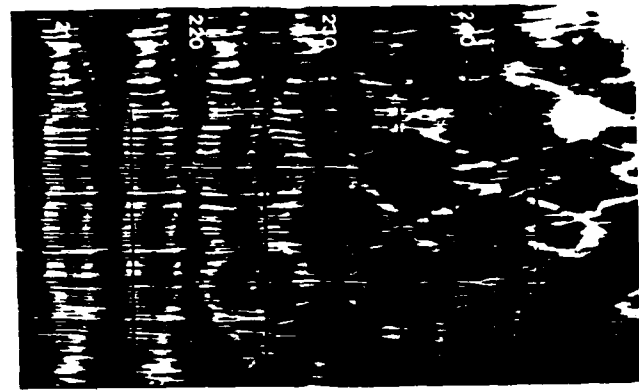


Figure 2. C-type breakdown. Same as Fig. 1 except u' at Branch II is approx. 0.3%. At $R=1000$, $b=.15$, $b/a=0.67$.

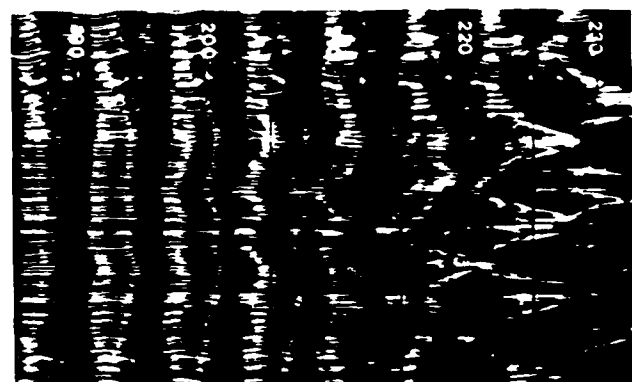


Figure 3. H-type breakdown. Same as Figure 1 except u' at Branch II is approx. 0.4%. At $R=1000$, $b=.32$, $b/a=1.46$.

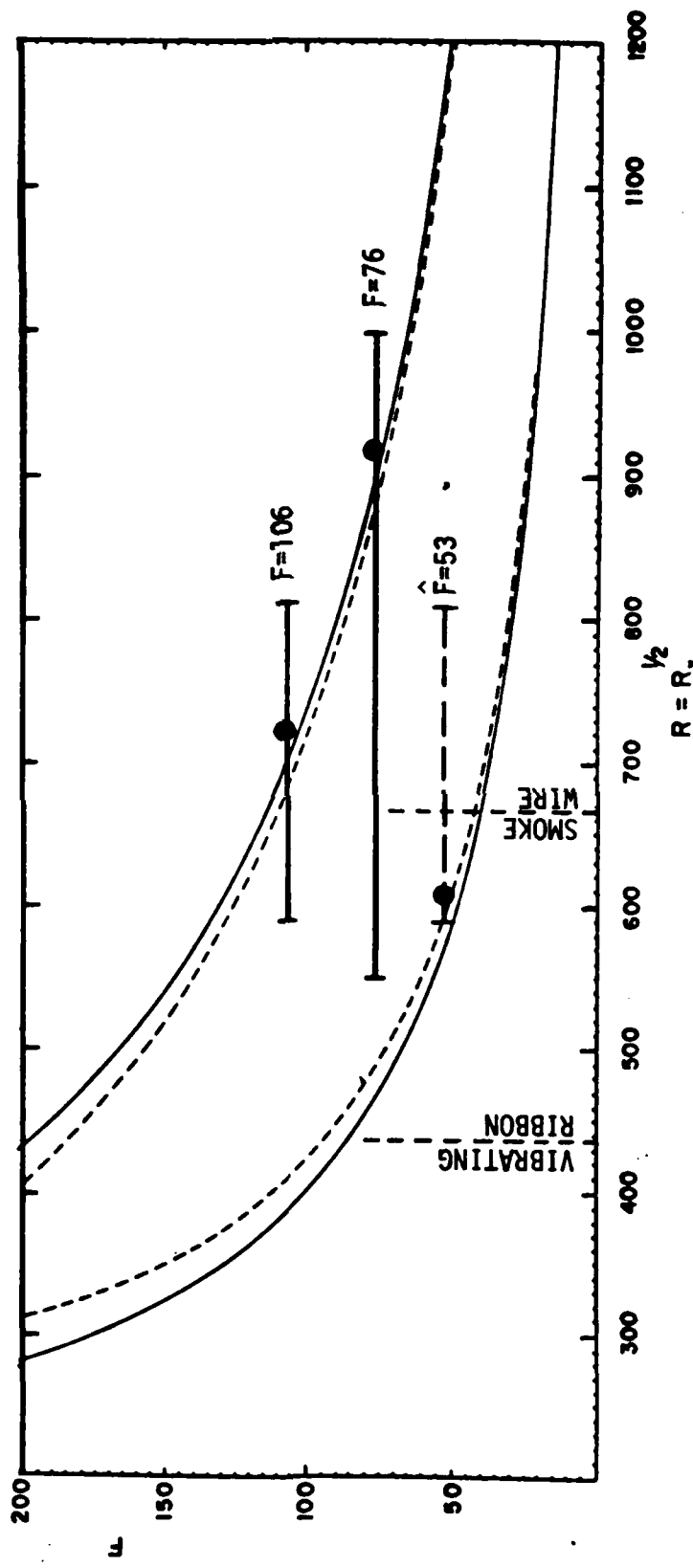


Figure 4. Neutral stability loop for Blasius boundary layer. The locations of the vibrating ribbon and the smoke wire are shown for $U_{\infty} = 7.5$ m/s. The range over which measurements are taken at $F=76$ and 106 is shown. The solid symbols are the experimentally determined neutral stability points at $u=0.4$.

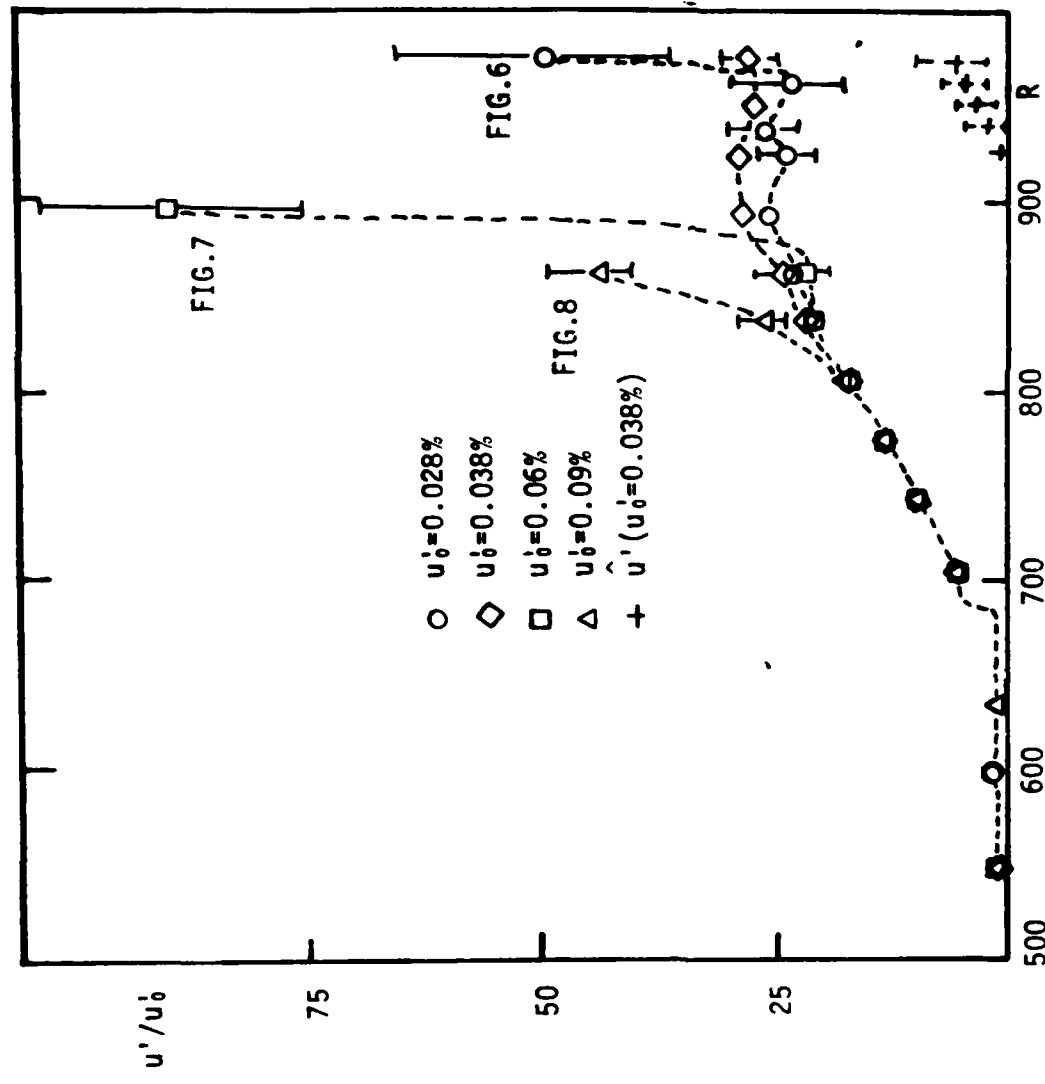


Figure 5. Normalized disturbance amplitude as a function of Reynolds number for naturally occurring subharmonics. u'_0 is the reference amplitude at $R=550$. Measurements made at $U=0.4$.

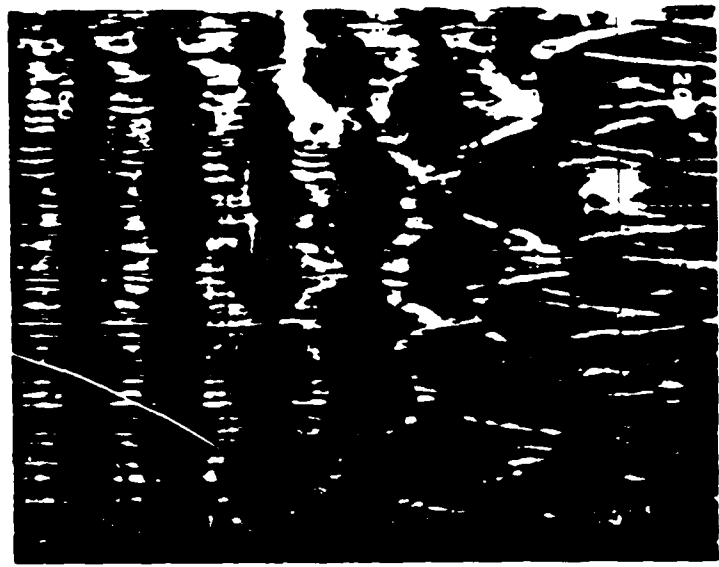


Figure 6. C-type breakdown at conditions of Fig. 5.

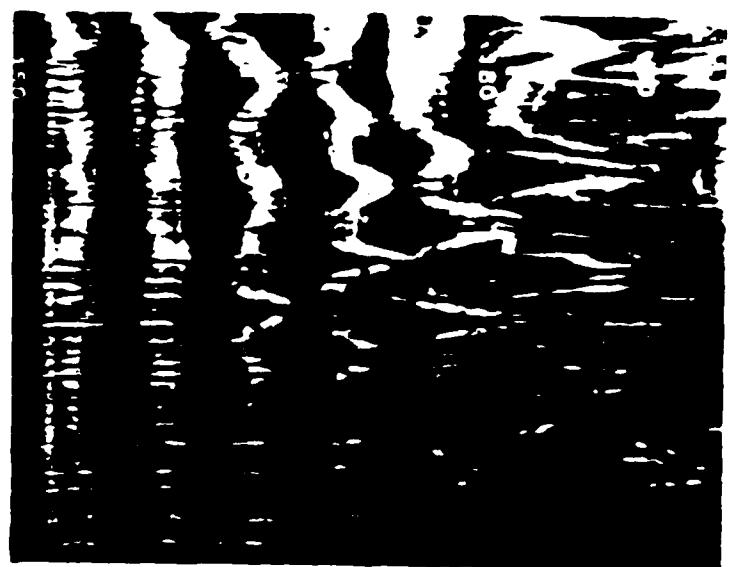


Figure 7. H-type breakdown at conditions of Fig. 5.

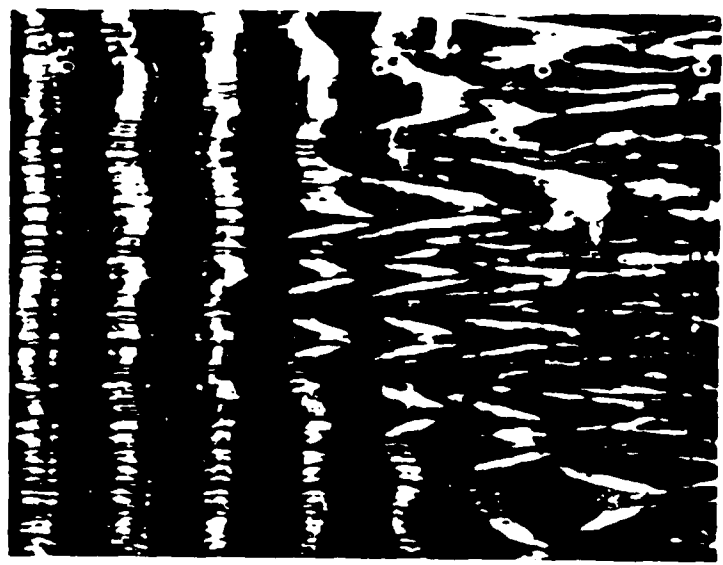


Figure 8. K-type breakdown at conditions of Fig. 5.

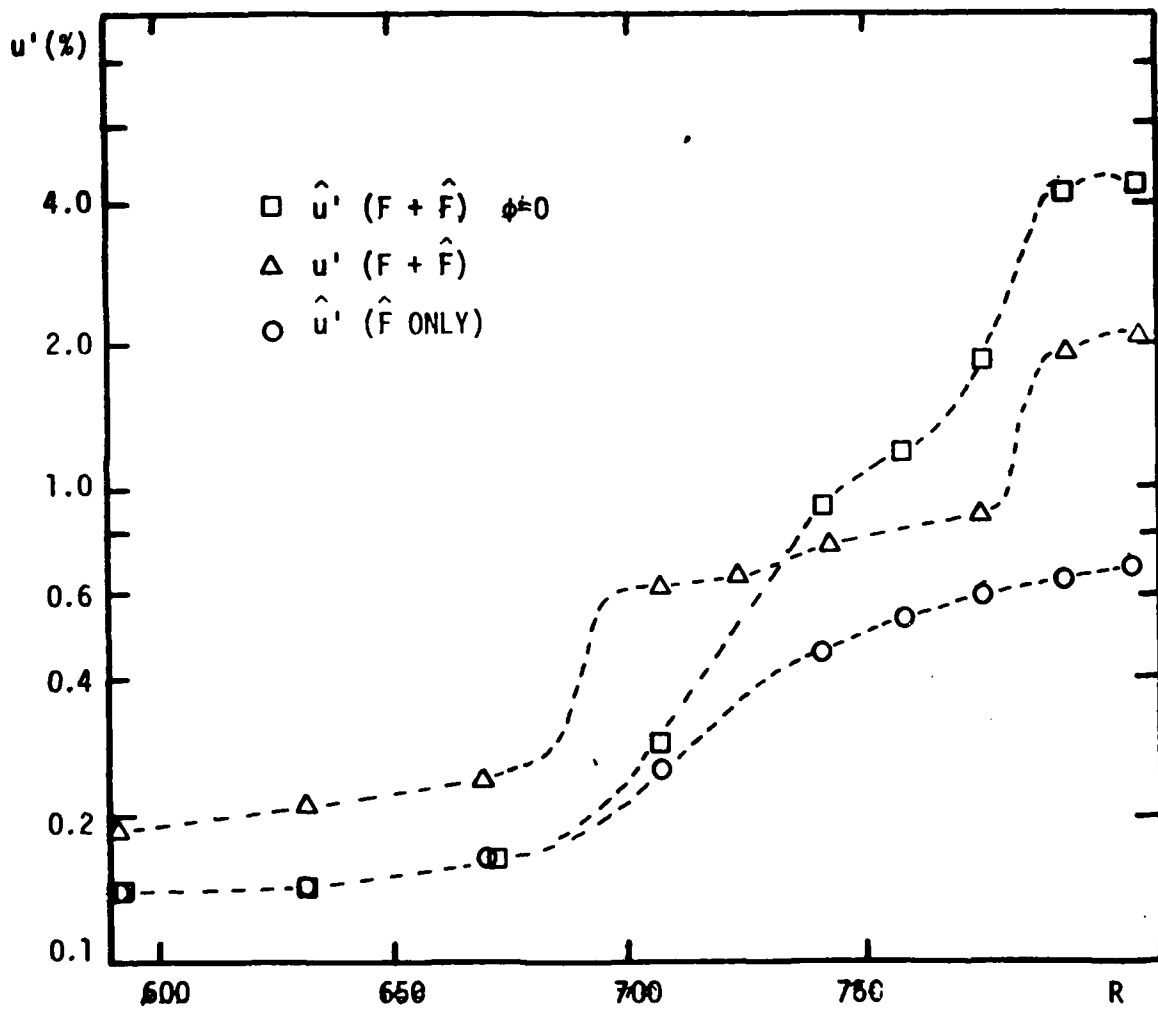


Figure 9. Disturbance amplitude as a function of R for controlled subharmonic in phase with fundamental. Measurements at $u=0.39$, $z=-2\text{cm}$.

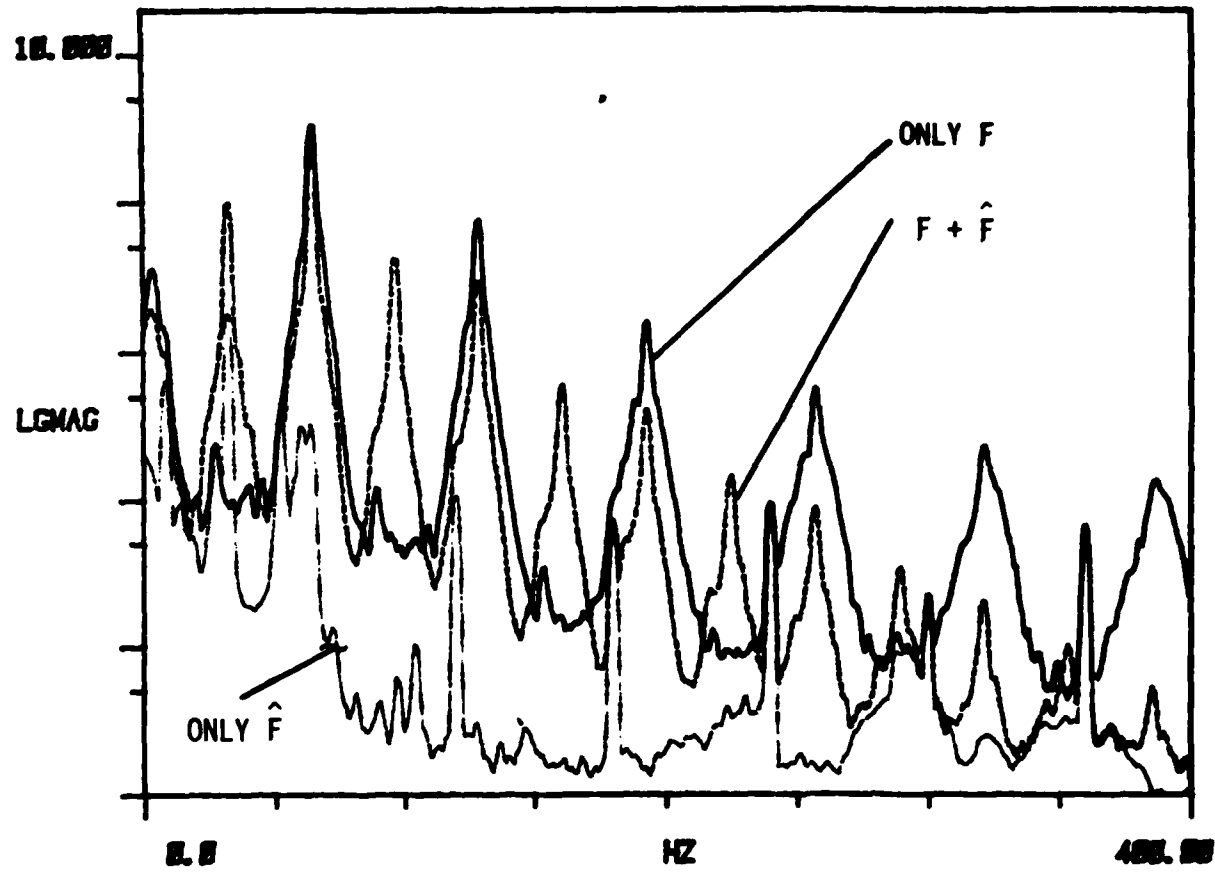


Figure 10. Spectra of disturbances (square root of autospectrum) at R=775 for three cases of input disturbances.

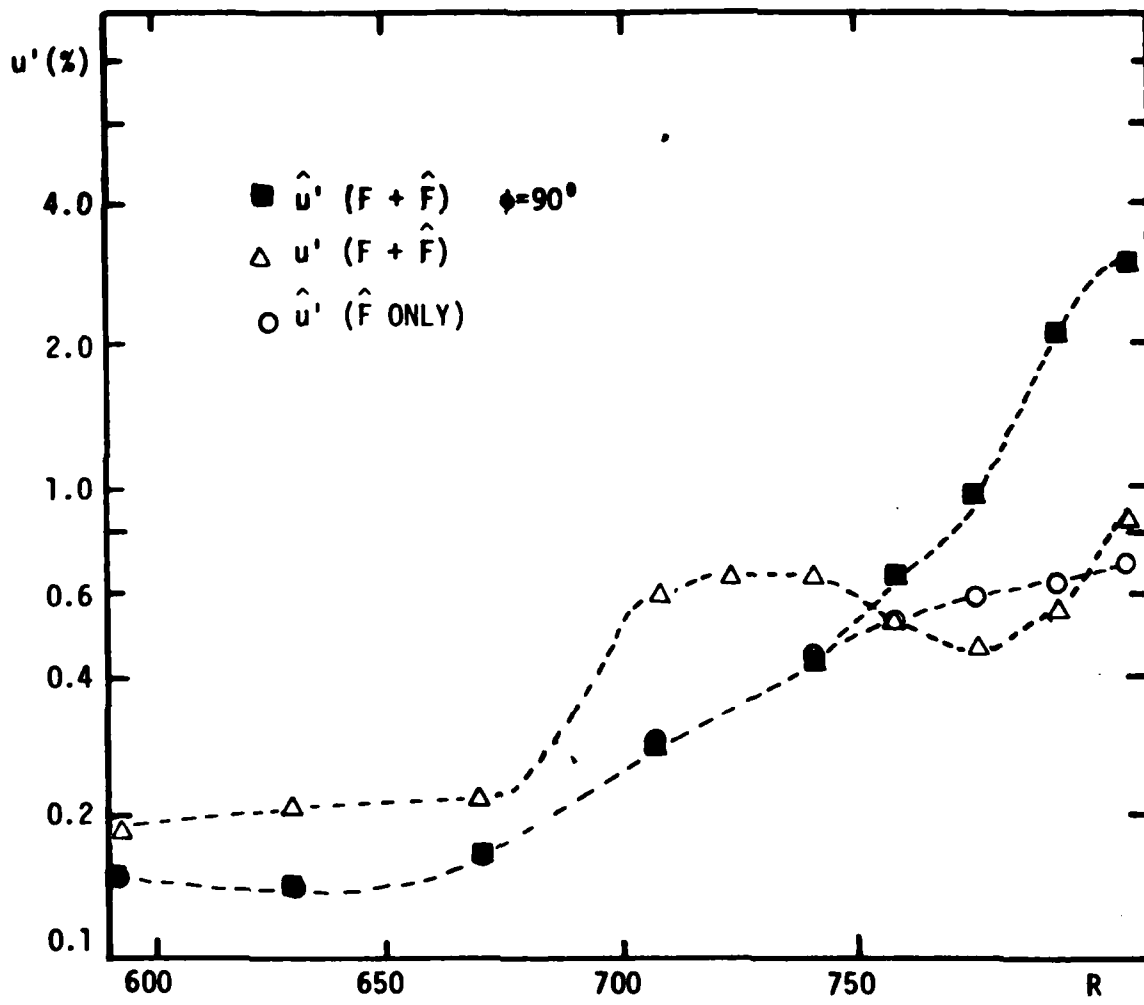


Figure 11. Disturbance amplitude versus R . Same conditions as Fig. 9 except the phase between fundamental and subharmonic is initially 90° .

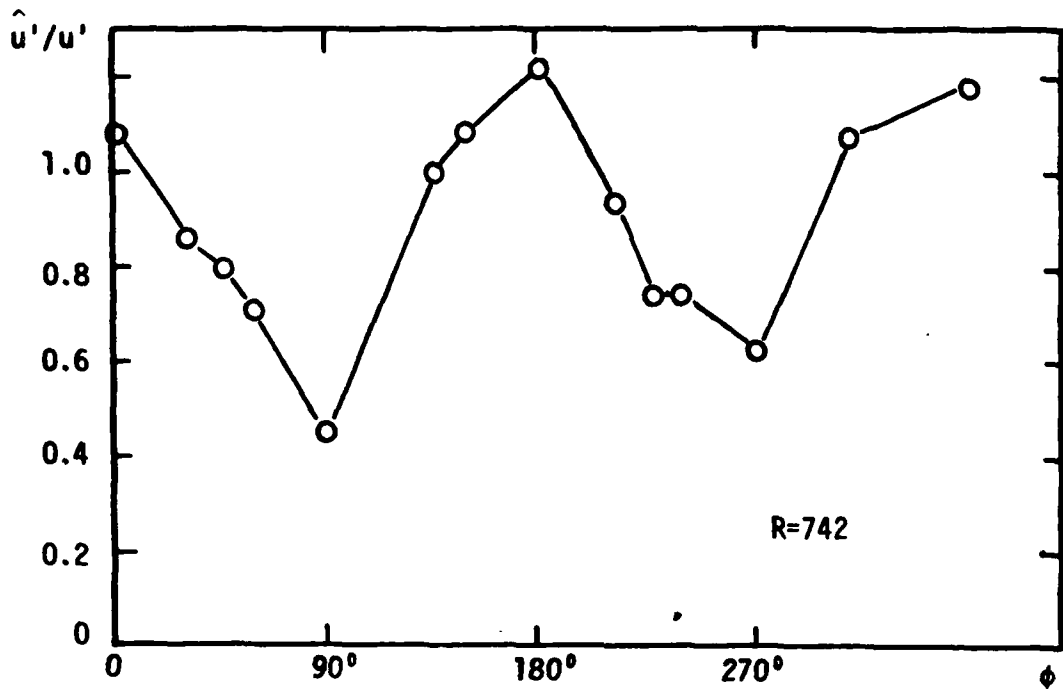


Figure 12a. Relative amplitude of the subharmonic as a function of initial relative phase. Measurements at $u=0.39$, $z=+2$ cm, and $R=742$.

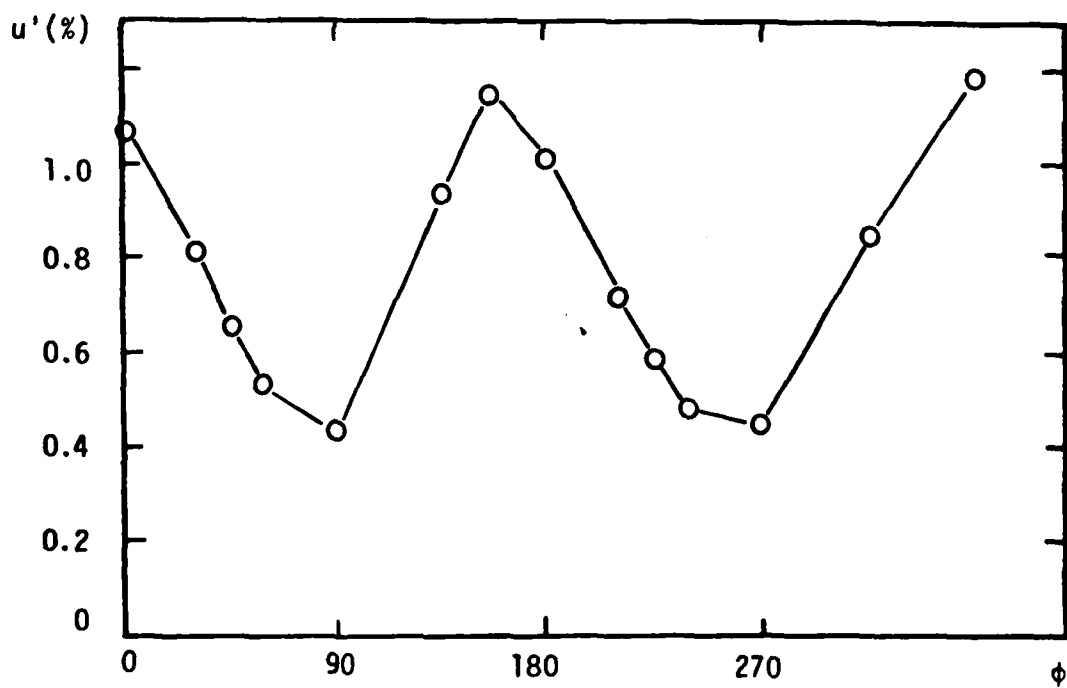


Figure 12b. Amplitude of fundamental as a function of initial relative phase. Same conditions as Fig. 12a.

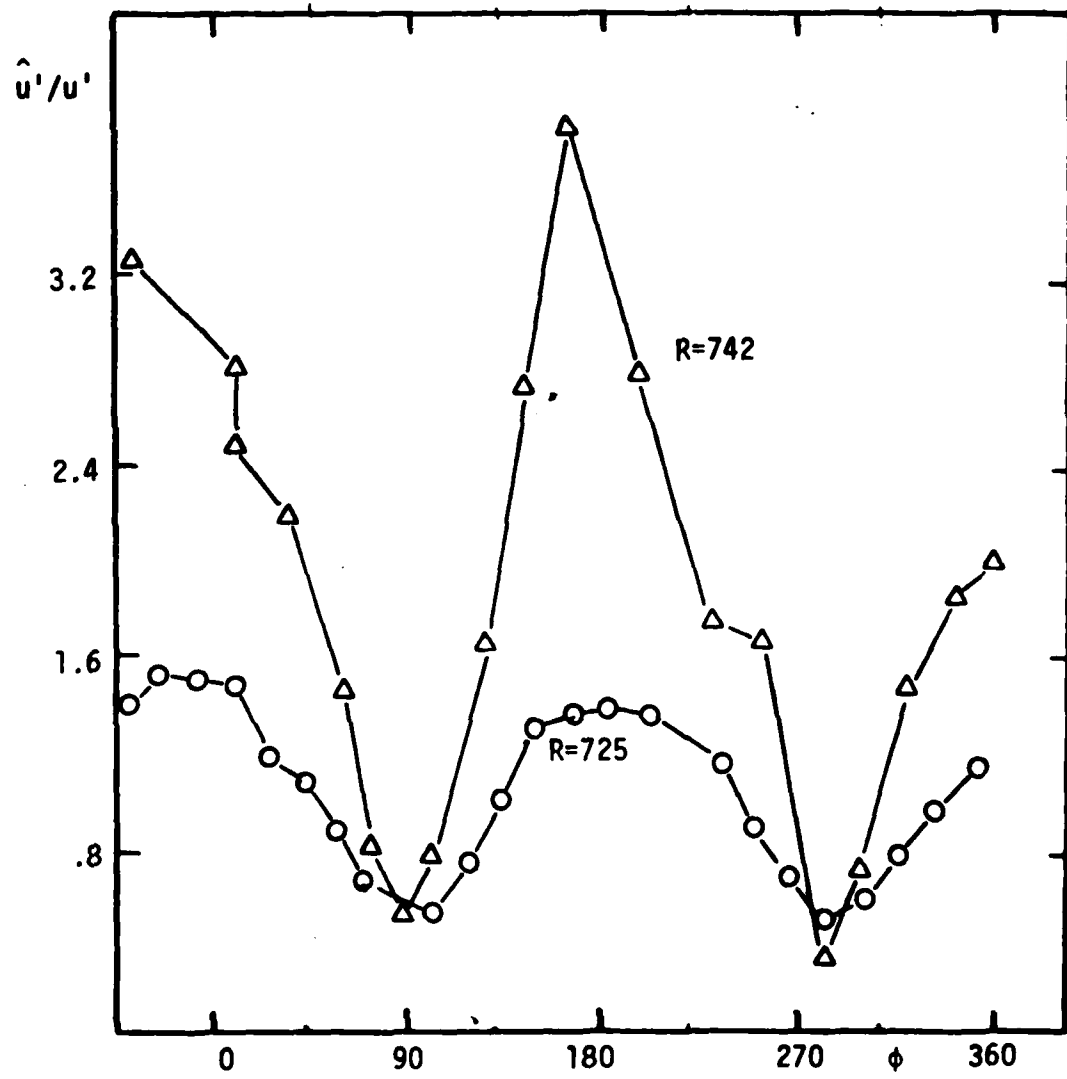


Figure 13. Relative amplitude of the subharmonic as a function of initial relative phase at $R=725$ and $R=742$ ($z=-2$ cm).

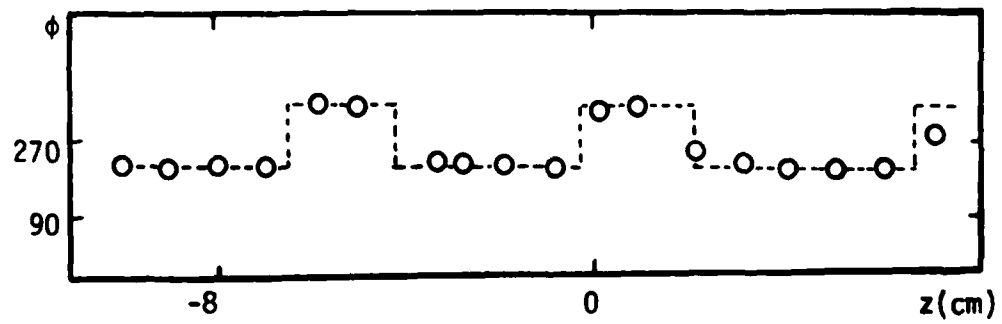
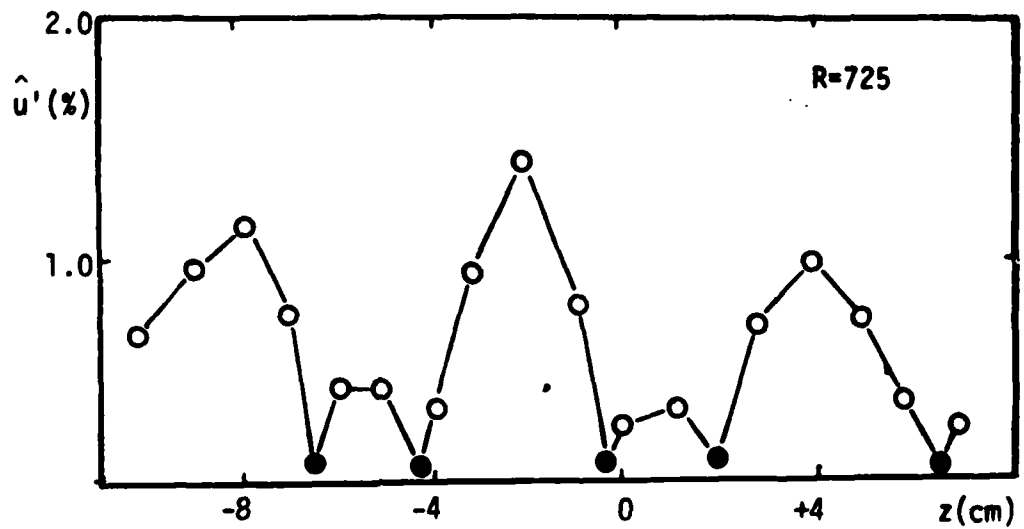


Figure 14. Amplitude and phase of subharmonic as a function of spanwise location. Solid symbols show locations of phase shift. ϕ is the actual phase of the subharmonic.

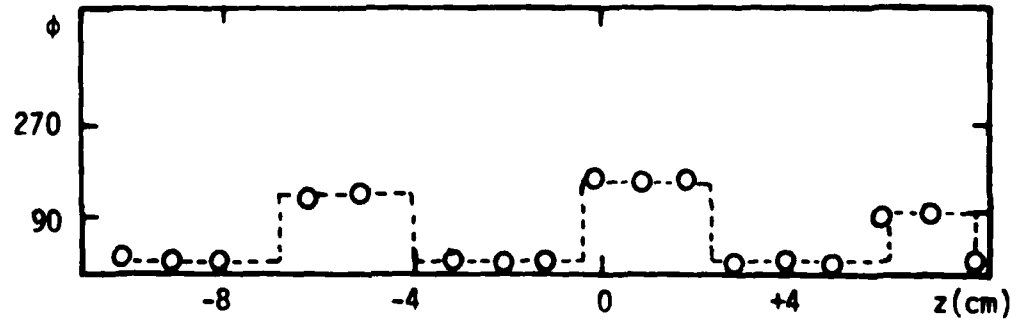
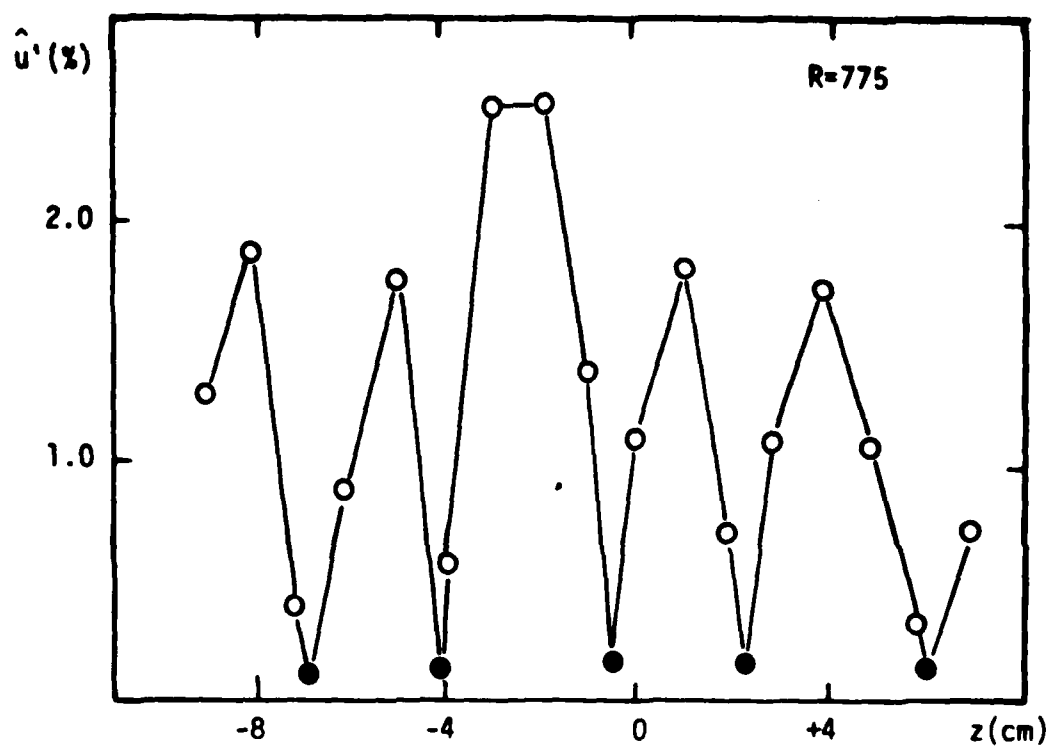


Figure 15. Same as Fig. 14 except at $R=775$.

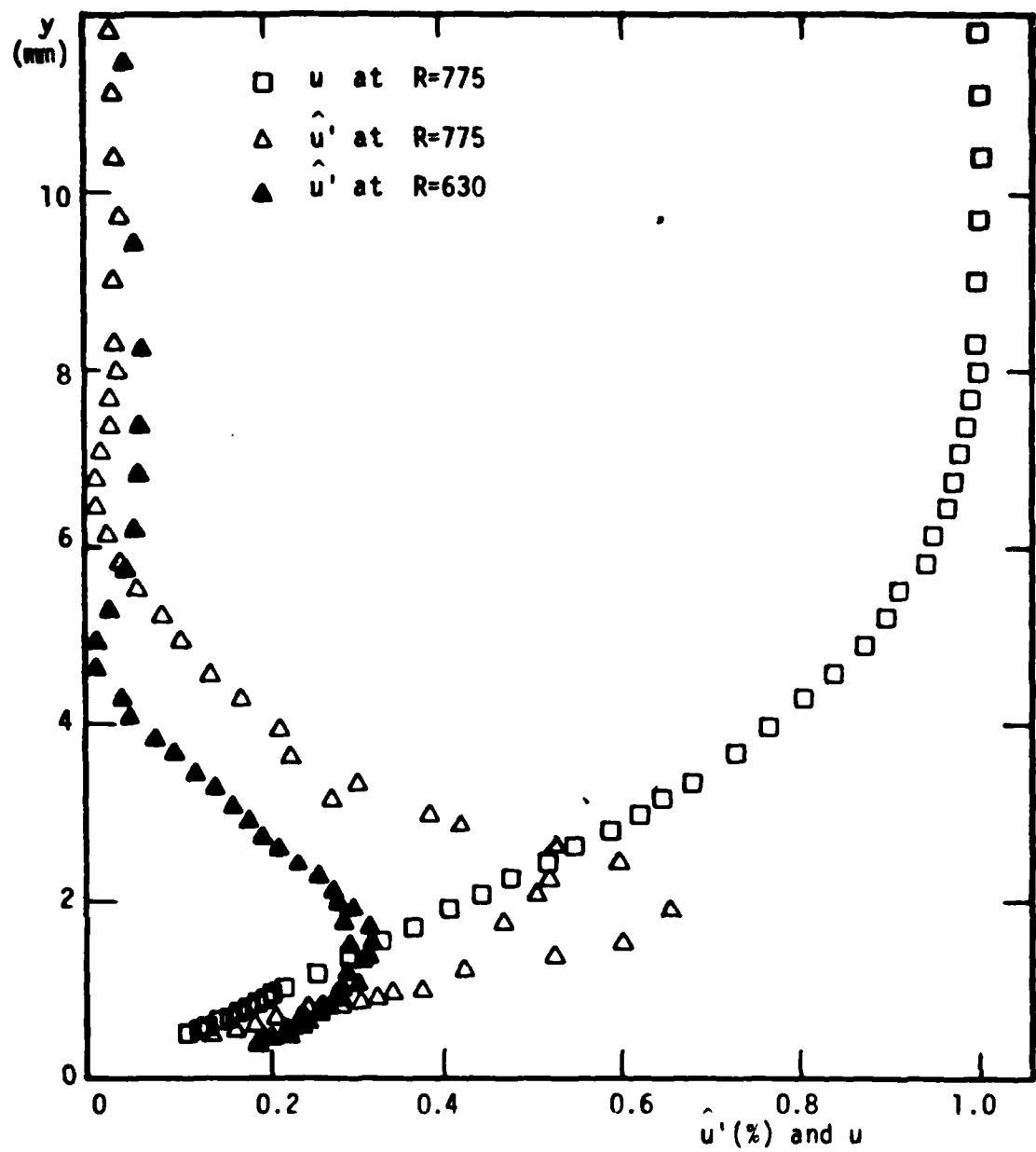


Figure 16. Velocity distributions through the boundary layer.
 U' in $\frac{1}{2} U_\infty$.

E A N D

5 — 8 7

D T / C